Dyes and Pigments 84 (2009) 121–127

Contents lists available at ScienceDirect

Dyes and Pigments

journal homepage: www.elsevier.com/locate/dyepig

# Highly bright and photostable cyanine dye-doped silica nanoparticles for optical imaging: Photophysical characterization and cell tests

Ivana Miletto [a,d,*], Alessandra Gilardino [c,d], Pollyanna Zamburlin [c,d], Simona Dalmazzo [c,d], Davide Lovisolo [c,d], Giuseppe Caputo [b,d], Guido Viscardi [a,d], Gianmario Martra [b,d]

[a] Università degli Studi di Torino, Dipartimento di Chimica Generale e Chimica Organica, Corso Massimo d'Azeglio 48, 10125 Torino, Italy
[b] Università degli Studi di Torino, Dipartimento di Chimica Inorganica, Fisica e dei Materiali, Via Pietro Giuria 7, 10125 Torino, Italy
[c] Università degli Studi di Torino, Dipartimento di Biologia Animale e dell'Uomo, Via Accademia Albertina 13, 10123 Torino, Italy
[d] NIS Centre of Excellence, Università di Torino, Via P. Giuria 7, 10125 Torino, Italy

ARTICLE INFO

*Article history:*
Received 26 March 2009
Received in revised form
13 July 2009
Accepted 14 July 2009
Available online 21 July 2009

*Keywords:*
Cyanine dye
Fluorescent hybrid silica nanoparticles
Optical imaging
Neuronal survival
Internalization

ABSTRACT

Spherical silica nanoparticles containing fluorescent trimethine indocyanine dyes ($\lambda_{abs}$ = 547 nm, $\lambda_{em}$ = 570 nm) were prepared using a water-in-oil microemulsion method. The nanoparticles were of ~50 nm diameter and were almost monodispersed in aqueous solution at pH 5.5. Entrapment of dye molecules in the silica matrix stabilised photoemission over several hours of continuous irradiation. The photoemission intensity of the indocyanine was increased 13-fold over that recorded in solution. As each nanoparticle contained ~110 dye molecules, the photoemission brightness of each particle was enhanced by three orders of magnitude. The fluorescent nanoparticles have been tested as imaging tools in *in vitro* tests. As an example of non-macrophagic cells, a highly differentiated neuronal cell line (GT1-7) was used and the results showed that the prepared nanoparticles can be incorporated into these cells with no apparent toxicity for up to three days.



## 1. Introduction

One of the main tasks of recent research in diagnostics and cellular imaging is the development of highly luminescent and photostable biolabelling agents [1–4]. Different types of fluorescent markers have traditionally been used for imaging purposes [5], but organic fluorophores are the most exploited, because of the large number of commercially available molecules that display interesting photophysical features as well as the possibility of tuning such fluorophores for more effective applications. Whilst such molecules are versatile and easy to use, they present several limitations, such as photodegradation and high sensitivity to environmental factors [1,6–8]. Furthermore, it is well known that molecular fluorophores must usually be attached to biomolecules in a ~1:1 ratio, so as to avoid interference with the activity/binding specificity of the biomolecular moiety and concentration quenching of the fluorophore. Such a constraint actually results in a limitation of the intensity of the photoluminescence signal at the basis of the imaging detection.

As a consequence, there is a growing interest in the development of new kinds of biomarkers, characterized by high photostability, biocompatibility, easy handling and bioconjugation, minimal environmental effects (minimal or no changes in properties of both the biomarker and the biomolecule) and high photoemission intensity [9,10].

Quantum dots (QD) and fluorescent nanoparticles fulfil some of these requirements, such as high photostability and insensitivity to environmental factors [11,12]. QD of different sizes and surface functionalisation are commercially available, and although there is a great number of publications about their use in *in vitro* applications [13], there are contrasting views about their cellular toxicity [2,3,14]. To avoid cell damage or death, it seems to be necessary to surround QD with a biocompatible shell, such as silica or a polymer [12,15].

Dye-doped silica nanoparticles (NPs) have also attracted interest, because the entrapment of the organic molecules within the silica matrix should result in an increase of the quantum yield of the fluorophores, thus enhancing the overall brightness of the fluorescent probe. Furthermore, the silica matrix preserves the encapsulated fluorophore from environmental factors that can

* Corresponding author. Present address: Università degli Studi di Torino, Dipartimento di Chimica IFM, Unit at the Centre for Innovation, Via Quarello 11/A, 10135 Torino, Italy. Tel.: +39 0116708384; fax: +39 0116707855.
*E-mail address:* ivana.miletto@unito.it (I. Miletto).

0143-7208/$ – see front matter © 2009 Elsevier Ltd. All rights reserved.
doi:10.1016/j.dyepig.2009.07.004

affect the optical performance, such as oxidation by reaction with $O_2$ present in air or dissolved in water. This kind of hybrid material can be easily prepared by hydrolysis and condensation of a silica precursor via sol–gel (Stöber method) or reverse microemulsion synthesis, the latter resulting in the production of nanoparticles more homogeneous both in shape and size [16,17]. In this respect, recent publications refer to silica NPs of diameter <100 nm, varying from 20–30 to 80 nm, doped with traditional dyes such as fluoresceine isothiocyanate (FITC), rhodamine 6G (R6G), 6-carboxyrhodamine, tetramethylrhodamine and RuII(bpy)$_3$ [18–22].

However, it is of interest to extend the investigation to other photoluminescent molecules, with different photophysical properties, such as indocyanines, that are characterized by a significant quantum yield (around 0.05–0.1), and exhibit absorption and emission wavelength (hereafter, $\lambda_{abs}$ and $\lambda_{em}$, respectively) that can be tuned by changing the length of the polymethine chain [23]. For our study, we selected a trimethine indocyanine, with a $\lambda_{em} = 570$ nm (of interest because its fluorescence is more shifted towards to the red with respect to commonly used fluoresceins and rhodamines); the use of a cyanine dye emitting in the red region of the spectrum reduces the interference with the autofluorescence of biological samples. As for the preparation method, the silica-based NPs were prepared by microemulsion, resulting in a quite narrow size distribution, and the inclusion in NPs of both the cyanine molecules as such or conjugated with aminopropyltriethoxysilane (APTS) was tested. Dimension and dispersion of nanoparticles were assessed by dynamic light scattering (DLS) and transmission electron microscopy (TEM). The optical absorption and emission properties of the hybrid systems were then evaluated and compared to the dye in solution. In particular, the influence of the entrapment within the silica matrix on the fluorescence quantum yield and on the photostability of the dye was evaluated. Silica-based NPs have been used in a number of cell tests, but in most cases cell lines were of a macrophagic-like type. In our study, as an additional aspect of novelty, tests were performed with a highly differentiated neuronal cell line, GT1-7 cells, a consolidated neurosecretory model, not specialized for phagocytising behaviour [24].

## 2. Experimental section

### 2.1. Materials

*IRIS3* cyanine dyes (**I**) and *IRIS3NHS* (**II**) derivatives for subsequent conjugation with APTS were kindly provided by Cyanine Technologies S.r.l. (Torino, Italy). The cyanine employed contained a phthalimido group introduced by Cyanine Technologies as an amino-protecting group, which can be cleaved and used for conjugation with carboxylic acid in other kinds of applications. All other reagents and solvents were purchased by Sigma–Aldrich and used as received.

### 2.2. Methods

#### 2.2.1. Preparation of IRIS3/APTS conjugate (*III*)

Aminopropyltriethoxysilane (APTS) (46.00 μmol; 10 μl) was added to a solution of **II** in DMF (11.50 μmol; 500 μl). The mixture was stirred for 24 h at room temperature (r.t.) and monitored by TLC, until the complete disappearance of the spot of compound **II**, and by MS spectrometry, that confirmed the complete conversion of **II** in **III**. Finally, the product was separated from unreacted APTS through dilution in diethyl ether, yielding **III** as a free powder. ESI-ION TRAP $m/z = 834$ $[M\text{-}I]^+$.

Schemes of the structure of compound **I**, **II** and **III** are reported in Fig. 1.

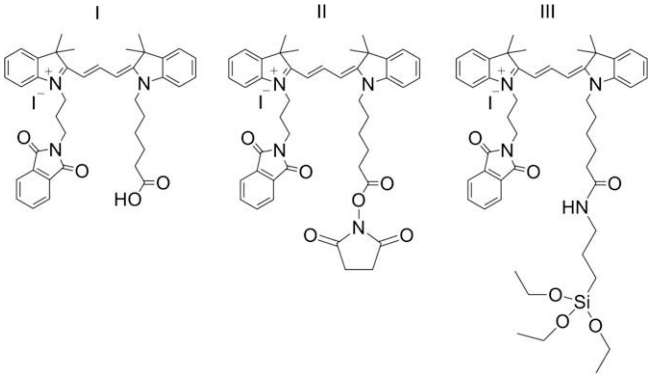


**Fig. 1.** Schemes of the structures of: IRIS3 (**I**), IRIS3NHS (**II**) and IRIS3/APTS conjugate (**III**).

#### 2.2.2. Preparation of silica-based nanoparticles

NPs were prepared in a W/O (water-in-oil) microemulsion, as reported by Santra et al. [22]. The microemulsion environment was formed by mixing cyclohexane (75 mL), *n*-hexanol (18 mL), *TritonX-100* (17.7 mL) and distilled water (5.4 mL). After stirring the microemulsion for 30 min, 0.2 mL (0.6 μmol) of **I** or **III** were added, and the mixture was further stirred for 10 min. Tetraethyl orthosilicate (TEOS) 1 mL (4.5 mmol) and $NH_4OH$ 0.7 mL (28–30%, 5.3 mmol) were then added and the reaction mixture was stirred at r.t. for 18 h and the ensuing nanoparticles were isolated from the suspension by adding acetone, followed by centrifuging and washing several times with ethanol and water to remove surfactant and unreacted species. The slurry of NPs so obtained was then re-suspended in distilled water (final pH = 5.5), resulting in suspensions that were stable for ca. 30 days.

#### 2.2.3. Dynamic light scattering (DLS)

The dispersion of NPs in suspensions was evaluated by DLS analyses, performed with a ALV-5000 Multiple Tau Digital Correlator equipped with a thermostated cell holder and a He–Ne laser operating at 633 nm. Hydrodynamic radii (HR) were obtained from cumulative fits of the autocorrelation functions. Samples were prepared by sonication of water suspension and progressive dilution to stay in the instrumental linearity range.

#### 2.2.4. Transmission electron microscopy (TEM)

TEM observations were performed on a JEOL 2000 EX instrument operating at 200 KV. For the measurements, a droplet of the suspensions of NPs was spread on a copper grid coated with a perforated carbon film, and then the liquid was allowed to evaporate slowly, to limit the agglomeration of NPs. The histogram of the size distribution of NPs was obtained by measuring ca. 300 particles, and the mean particle diameter (dm) was calculated as $d_m = \sum d_i n_i / \sum n_i$, where $n_i$ was the number of particles of diameter $d_i$. The results are indicated as ($d_m \pm$STDV).

#### 2.2.5. Gas picnometry

Gas picnometry was employed for the measurement of the density of the prepared NPs by using a Micromeritics ASAP2020 instrument.

#### 2.2.6. UV–Vis absorption and photoluminescence spectroscopy

Absorption UV–Vis spectra were collected with a Shimadzu PharmaSpec UV1700. Photoemission steady state spectra were acquired with a Horiba Jobin Yvon Fluorolog3 TCSPC spectrofluorimeter equipped with a 450 W Xenon lamp and a Hamamatsu R928 photomultiplier.

*2.2.7. Cytotoxicity tests*

GT1-7 neuronal cells [25,26] were seeded on uncoated plastic dishes (Falcon, Becton Dickinson, Franklin Lakes, NJ, USA), at a density of 30.000 cells/cm$^2$ and maintained in Dulbecco's Modified Eagle's medium (DMEM) supplemented with either 10% or 0.5% heat-inactivated fetal calf serum (FCS, Lonza, Basel, Switzerland), 50 μg/mL gentamycin and 2 mM glutamine, at 37 °C, in a humidified atmosphere of 5% $CO_2$ in air. 10% FCS is the standard culture condition used in order to maintain cell proliferation; 0.5% FCS (or serum deprivation) is the concentration commonly adopted to induce a differentiated phenotype in GT1-7 cells. Cells were incubated with a 20 μg/mL NPs suspension 24 h after seeding. Cytotoxicity was evaluated by counting cells with a Burker chamber at 24 and 72 h after incubation with NPs and in control conditions (no NPs added to the medium). Data (number of cells per cm$^2$) were expressed as mean ± STDV. Three independent experiments in triplicate for each condition were carried out.

One-way ANOVA and post hoc Bonferroni tests [27] were performed to evaluate statistically significant differences within the data.

*2.2.8. Internalization tests*

GT1-7 cells were seeded on glass microscope coverslips (Marienfeld, Lauda-Königshofen, Germany), at a density of 30.000 cells/cm$^2$ in 10% FCS DMEM for 24, 48 and 72 h in the presence of a 20 μg/mL suspension of IRIS3NPs. Cells were fixed in 4% PAF for 20 min at room temperature, permeabilized with 0.01% Triton-PBS, then blocked with 10% normal goat serum and incubated overnight at 4 °C with a monoclonal anti-β–Tubulin III (anti-β–TubIII) antibody (1:500). The reaction was developed with a goat biotinylated anti-mouse IgG (Vector Laboratories, Burlingame, CA; 1:200) and detected with the Avidin–FITC complex (Vector Laboratories; 1:400).

Images (1.024 × 1.024 pixel, 16-bit grey scale) were acquired by means of a Olympus Fluoview 200 laser scanning confocal microscope (Olympus America Inc., Melville, NY, USA) with a 100× objective, at excitation wavelengths of 568 and 488 nm. For each field, both the fluorescence and the differential interference contrast (DIC) images were acquired. Images obtained were analyzed with ImageJ, a public domain Java image-processing software tool [28].

## 3. Results and discussion

### 3.1. Dispersion and shape & size of NPs

The size and dispersion of NPs in the suspension obtained at the end of the preparation procedures were checked by DLS (Fig. 2A). The distribution of hydrodynamic radii (HR) appeared dominated by a peak centred at ca. 25 nm, broadened towards larger radii and with an additional weak component at ca. 180 nm. As for the shape of the particles, a representative TEM image of NPs is shown in Fig. 2B, where well shaped spherical particles can be observed, in close contact and/or partially overlapped each other. The statistical evaluation of the size of the spheres resulted in the histogram reported in Fig. 2C, spread over a quite narrow size range, from 45 to 55 nm, from which a mean size of 50 ± 2 nm was calculated.

Noticeably, such a mean size fits quite well with the maximum of the distribution of the HR obtained by DLS. Furthermore, as no particles larger in size than 55 nm were observed, it can be concluded that the objects exhibiting HR larger than such values should have been produced by spherical particles of 50 nm in size (hereafter: "primary particles") partially merged to form some aggregates. The vertical line on the curve in Fig. 2A is the threshold HR value, ca. 55 nm (the largest size of primary spherical particles observed by TEM), between single primary spherical particles and

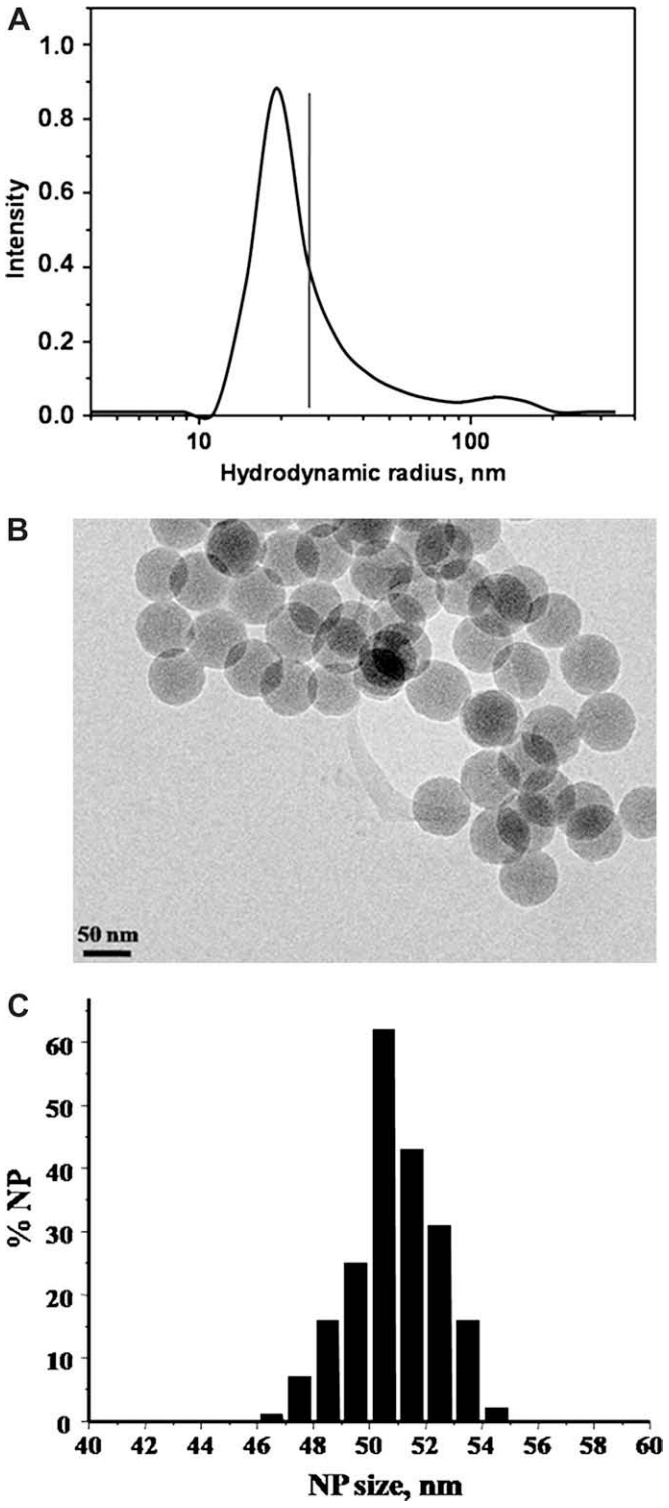


**Fig. 2.** Dispersion and shape/size of NPs. Section A: distribution of HR obtained by DLS measurements performed on an aqueous suspension of NPs (1.0 mg/mL) at pH = 5.5; section B: representative TEM image of NPs; original magnification 40.000×; section C: histogram of the size distribution of the primary spherical particles.

their agglomerates. The integrated area below the HR profile on the left of such vertical line accounts for ca. 70% of the overall integrated area, indicating that single spherical NPs are the large majority. Furthermore, the merging among surface/volume of primary particles involved in agglomerates appeared quite limited

(TEM), allowing us to assume a sphere of 50 nm in diameter as the "basic unit" for the evaluation of a variety of properties of the system. On such a basis, as the density of the silica material prepared was ca. 2.2 g/cm$^3$ (equivalent to that of amorphous silica [29]), and having assessed by ICP MS a consumption of 90% of TEOS to produce NPs, it was possible to estimate the number of NPs obtained for each preparation (ca. $7.60 \times 10^{12}$ NPs/mg).

### 3.2. UV–Vis absorption and emission behaviour of NPs

The UV–Vis absorption and emission spectra of **III**, identical to those of compound **I** are reported in Fig. 3 (curves a and a′, respectively). The absorption profile is characterized by a main component at 547 nm, with a hypsochromic shoulder at 515 nm, while the photoemission exhibits an almost specular profile, with maximum at 570 nm and a shoulder at 600 nm.

The nature of visible absorption and emission of cyanine dyes can be explained by referring to what has been proposed for similar polymethine systems [30]. Several authors state that these bands are due to $\pi \rightarrow \pi^*$ transitions, with partial character of charge transfer, as the delocalization is extended to positively charged nitrogen atoms of the heterocyclic groups [31–34]. As for the origin of the two components in both the absorption and emission profile, a general consensus has not been reached in the literature yet. Some authors reported the possibility that they can be due to cis and trans isomers of the cyanine molecule [35]; on the other hand, the most recognized model correlates the main component and the hypsochromic shoulder with transitions occurring between the lowest vibrational level of the ground (excited) state and two different vibrational levels of the excited (ground) state [31,32,36,37a]. As for the NPs loaded with the cyanine (as such, **I**, or as APTS derivative, **III**), no **I** or **III** molecules were found in the supernatant over the NPs separated by centrifugation (spectrophotometric analysis), indicating that in both cases all dye molecules were associated to NPs. However, the use of **I** (cyanine molecules as such) was ineffective, as the dye underwent a complete leaching from NP by simply washing with ethanol. Conversely, the use of compound **III** resulted in coloured NPs fully resistant to repeated ethanol washing, indicating a firm interaction with the silica matrix. On the basis of the number of nanoparticles present in the amount of sample used (see Section 3.1) and of the number of **III** molecules employed, it was possible to calculate that each nanoparticle contained ca. 110 cyanine molecules. The excitation (the absorption profile) and emission features of the NPs loaded with **III** (hereafter NPs-**III**) are reported as curve b and b′, respectively, in Fig. 3. The absorption profile was obtained through the excitation mode because only the intensity of the photoluminescence signals appeared linearly dependent on the suspension concentration in the 0.0–2.1 mg/mL range explored (Supporting information, Fig. 1S), whereas such a linear dependence was absent in the case of the absorption spectra collected in the usual transmission mode, because of the more relevant effect of the light scattering by NPs.

The excitation spectrum of NPs-**III** was broader and exhibited significant differences in the relative intensity of the various components with respect to compound **III** in solution (Fig. 3b and a). It must be noticed that the excitation profile (Fig. 3b) appeared almost coincident with the absorption profile obtained in the diffuse reflectance mode on dry NPs-**III** properly diluted in pure silica in order to avoid possible inner filter effects. Such behaviour indicated that all types of molecular structure responsible for the absorption are also involved in the photoemission. By considering that many authors proposed that the structure of the absorption spectrum of cyanines is due to vibronic transitions, it can be proposed that in the present case the peculiar features of the absorption/excitation profile are due to a modification of the probability of transitions from the ground vibro-electronic state to different vibrational levels of the excited electronic state.

On the basis of the number of **III** molecules associated to each NP (see above), a solution of **III** and a suspension of NPs-**III** with the same amount of **III** molecules (corresponding to a molar concentration of $1.0 \times 10^{-6}$) were prepared. These two samples were used to assess the actual location of **III** molecules in NPs-**III**, and to compare the photoemission intensity of **III** when free in solution or associated with the NPs.

As for the first target, a photostability test was performed, because dye molecules accessible to molecular oxygen dissolved in the liquid medium were expected to be photo-oxidized to non-photoluminescent products. As a reference, the photoemission intensity at $\lambda_{max} = 570$ nm of a aqueous solution ($1.0 \times 10^{-6}$ M) of

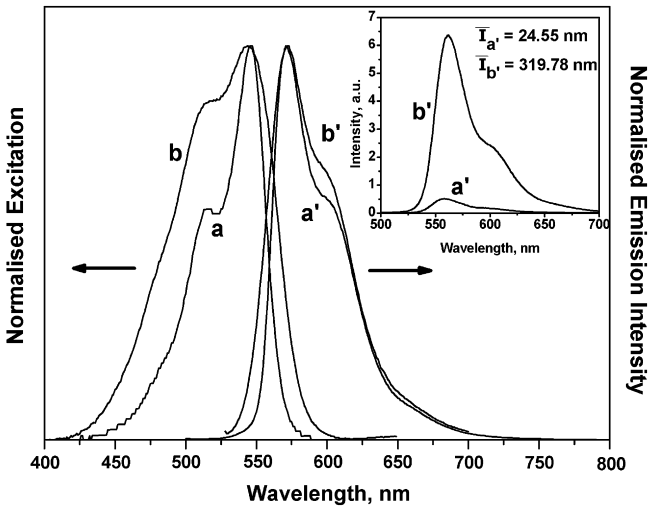


**Fig. 3.** Comparison between the electronic spectra (normalized to the maximum of the intensity) of dye (**III**) in solution ($1.0 \times 10^{-6}$ M) and of NPs-**III** in suspension (1.0 mg/mL, corresponding to $1.0 \times 10^{-6}$ M in **III**): a) absorption and a′) emission ($\lambda_{ex} = 500$ nm) spectra of **III**; b) excitation ($\lambda_{em} = 570$ nm) and b′) emission ($\lambda_{ex} = 500$ nm) spectra of NPs-**III**. Inset: comparison of the actual intensity of the photoemission spectra of the dye (**III**) solution (a″) NPs-**III** suspension (b″).

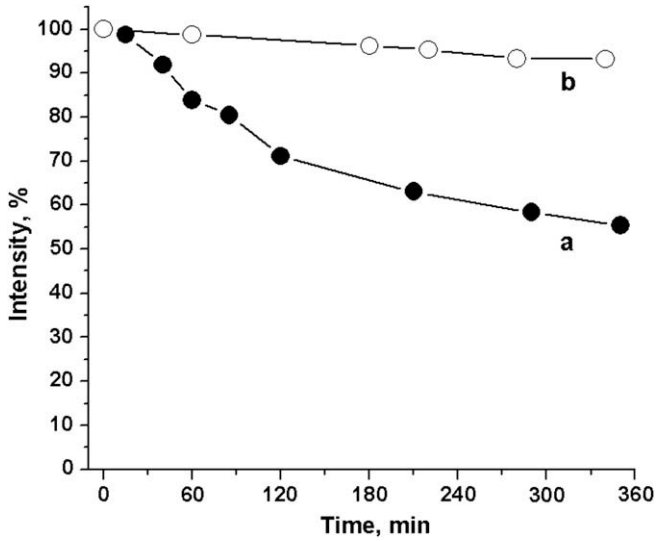


**Fig. 4.** Photoemission stability test, carried out by irradiating with at $\lambda_{ex} = 500$ nm: a) aqueous solution of **III**, $1.0 \times 10^{-6}$ M; b) aqueous suspension of NPs 1.0 mg/mL, corresponding to $1.0 \times 10^{-6}$ M in **III**).

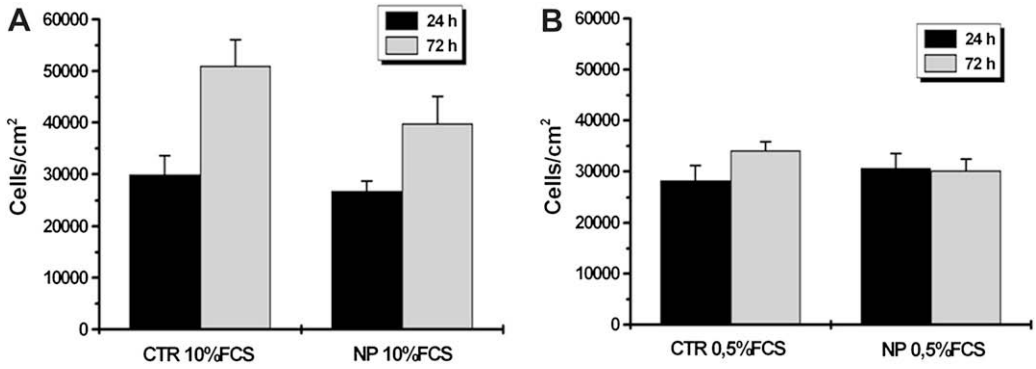


**Fig. 5.** Results of: section A) proliferation and section B) survival tests of GT1-7 cells cultured after addition of NPs-**III** (20 μg/mL). Both parameters were evaluated at 24 (black bars) and 72 h (grey bars).

**III** was monitored under continuous irradiation in the spectrofluorimeter, and a progressive decay down to ca. 55% of the initial value was observed (Fig. 4a). On the contrary, the irradiation of a NPs-**III** suspension (1.0 mg/mL, that should correspond to the presence of ca. $1.0 \times 10^{-6}$ mol of **III** per litre of suspension) over the same time resulted in a decrease of ca. 7% only of the initial intensity (Fig. 4b), indicating that the dye molecules should be encapsulated within the silica matrix, where reaction with oxygen is significantly hindered.

The photoluminescence spectra of fresh **III** solution and NPs-**III** suspension were then recorded and compared (Fig. 3, inset). The solution of **III** was kept in contact with air, because dissolved oxygen was expected to be quite ineffective as quenching agent towards fluorophores with lifetimes shorter than 5 ns [37b], as typically exhibited by cyanine dyes [38].

Noticeably, the integrated intensity of the signal emitted by the NPs-**III** suspension was ca. 13-fold that obtained for the solution of **III**. Because of the cyanine equimolar character of the two systems, it can be concluded that the higher emission intensity obtained for the suspension should result from a significant increase of the quantum yield of dye molecules entrapped in the silica NPs. This increase in quantum yield should be ascribed to the decreased occurrence of non-radiative relaxation processes in favour of the radiative ones, because of the loss of mobility. It is of interest to notice that such a behaviour appeared: i) opposite to what reported in previous works dealing with silica NPs functionalized with pyrene-APTS [39] or FITC-APTS [40] conjugates, where the occurrence of self-quenching due to interactions between fluorescent molecules was observed; ii) in agreement with what recently found by Larson et al. [41] for silica NPs containing rhodamine molecules (previously conjugated with APTS), where the emission enhancement per dye molecule was attributed to a combined enhancement in the radiative decay rate and decrease of the non-radiative one, in the absence of observable energy transfer between neighbouring dyes.

As each of our NPs-**III** contains ca. 110 cyanine molecules, it can be then concluded that the overall brightness enhancement of each particle relative to the free dye, i.e. the product of the number of dye molecules inside the particle and the relative quantum efficiency enhancement of the encapsulated dye, reaches a value of ca. 1000-fold. On the basis of a "brightness enhancement per $nm^3$", such a gain factor still appeared 10-fold higher than that found by Larson et al. for their rhodamine/APTS-NPs [41].

The origin of such a large gain in the emission intensity obtained in the present case might result from a higher dispersion of the **III** adducts within the silica matrix with respect to rhodamine. Further investigations to highlight this point are in progress.

### 3.3. Cell tests

To assay the potential toxicity of the NPs-**III**, GT1-7 cells were cultured in normal medium with or without the NPs-**III** at

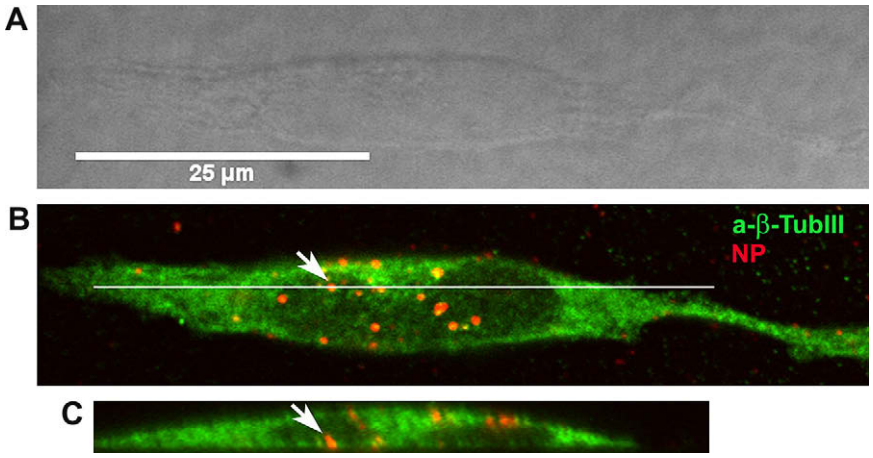


**Fig. 6.** DIC (panel A) and fluorescence (panels B, C) images of a GT1-7 cell incubated for 24 h with NPs-**III** (20 μg/mL) (red), and labelled with anti-β–TubIII antibody (green). Both the single focal plane (panel B) and the virtual section (panel C) along the horizontal white line in B show that NPs-**III** are incorporated into GT1-7 cells (white arrows). Scale bar: 25 μm. (For interpretation of the references to colour in this figure legend, the reader is referred to the web version of this article.)

a concentration of 20 μg/mL. Two conditions were adopted in order to evaluate the effect of NPs-**III** both on the proliferation and on the survival of this neuronal cell line: 10% FCS and 0.5% FCS, respectively. Cell numbers in the two conditions were evaluated after 24 and 72 h of incubation with (NP) or without (CTR) NPs-**III** suspension. Fig. 5A and B show that the hybrid system does not affect either the proliferative state or the survival of GT1-7 cells.

Internalization and subcellular localisation of NPs-**III** in GT1-7 cells were determined by labelling cells with a cytoplasmic antibody (anti-β–TubIII) after 24, 48 and 72 h of incubation in the presence of NPs-**III**. Images were analyzed performing a confocal *xyz*-acquisition (*z*-spaced at 0.2 μm) and 3D reconstructions with ImageJ software.

Fig. 6A shows the DIC image of a typical GT1-7 cell incubated for 24 h with NPs-**III** which reveals a normal morphology if compared to cells cultured under control conditions (no incubation with NPs-**III**, data not shown). A single focal plane of a 3D reconstruction of the same field displays a green cytoplasmic staining due to the anti-β–TubIII antibody and red spots corresponding to large aggregates of NPs-**III** (Fig. 6B). To better understand the actual localisation of internalized NPs-**III**, virtual sections in the *z*-plane of the *xyz*-acquisition were performed. Fig. 6C is an example of virtual section corresponding to the horizontal white line shown in Fig. 6B. Arrows (Fig. 6B and C) indicate that NPs-**III** are clearly incorporated in GT1-7 cells after 24 h of incubation. The same results have been obtained with longer incubation times up to 72 h (Supporting information, Fig. 2S).

## 4. Conclusions

The preparation method resulted in the formation of hybrid fluorescent dye-silica NPs, mainly as single spherical particles. The functionalisation with cyanine **I** resulted from the preliminary conjugation with APTS (compound **III**). In such a way, the dye molecules are obtained encapsulated within the silica matrix, with consequent significant improvement of photostability and photoluminescent intensity. As for the latter, on the basis of the estimated number of **III** molecules per NP, each NP-**III** should exhibit a ca. 1000-fold brightness enhancement relative to the free dye.

Biological tests showed that neuronal cells can survive and proliferate for days in the presence of a suspension of these particles and that, even more interestingly, NPs can be incorporated into the cells even without any specific surface functionalisation. This finding, together with the assessed high photostability and overall brightness enhancement provides evidence of their potential use as bright and non toxic markers for long lasting monitoring of the behaviour of differentiated cells in culture.

## Acknowledgments

This work has been carried out in the frame of the Nanomat-ASP project (Docup 2000–2006, Linea 2.4a). Authors are also grateful to Fondazione San Paolo for the financial support to NIS. Prof. V. Maurino (Department of Analytical Chemistry & NIS Centre of Excellence) and Dr. O. Russo (Micromeritics Italia S.r.l.) are acknowledged for assistance in DLS measurements and gas picnometry, respectively.

## Appendix. Supporting information

Supplementary data associated with this article can be found, in the online version, at doi:10.1016/j.dyepig.2009.07.004.

## References

[1] Sharma P, Brown S, Walter G, Santra S, Moudgil B. Nanoparticles for bioimaging. Adv Coll Interface Chem 2006;123(126):471–85.
[2] Medintz IL, Tetsuo Uyeda H, Goldman ER, Mattoussi H. Quantum dot bioconjugates for imaging, labelling and sensing. Nat Mater 2005;4(6):435–46.
[3] Michalet X, Pinaud FF, Bentolila LA, Tsay JM, Doose S, Li JJ, et al. Quantum dots for live cells, in vivo imaging, and diagnostics. Science 2005;307(5709):538–44.
[4] Wang L, Zhao W, Tan W. Bioconjugated silica nanoparticles: development and applications. Nano Res 2008;1(2):99–115.
[5] Mason WT. Fluorescent and luminescent probes for biological activity. 2nd ed. London: Academic Press; 1999.
[6] Zhang J, Campbell RE, Ting AY, Tsien RY. Creating new fluorescent probes for cell biology. Nat Rev 2002;3:906–18.
[7] Waggoner A. Fluorescent labels for proteomics and genomics. Curr Opin Chem Biol 2006;10(1):62–6.
[8] Dähne S, Resch-Genger U, Wolfbeis OS. Near-infrared dyes for high technology applications. NATO ASI series 3. High technology, vol. 52. Dordrecht, The Netherlands: Kluwer Academic Publishers; 1998.
[9] Hermansson G. Bioconjugate techniques. 2nd ed. Academic Press; 2008.
[10] Tansil NC, Gao Z. Nanoparticles in biomolecular detection. Nanotoday 2006;1(1):28–37.
[11] Yan J, Estévez MC, Smith JE, Wang K, He X, Wang L, et al. Dye-doped nanoparticles for bioanalysis. Nanotoday 2007;2(3):44–50.
[12] Resch-Genger U, Grabolle M, Cavaliere-Jaricot S, Nitschke R, Nann T. Quantum dots versus organic dyes as fluorescent labels. Nat Methods 2008;5(9):763–75.
[13] Biju V, Itoh T, Anas A, Sujith A, Ishikawa M. Semiconductor quantum dots and metal nanoparticles: syntheses, optical properties, and biological applications. Anal Bioanal Chem 2008;391(7):2469–95.
[14] Hardman RA. Toxicologic review of quantum dots: toxicity depends on physicochemical and environmental factors. Environ Health Perspect 2006;114(2):165–72.
[15] Selvan ST, Tan TT, Ying JK. Robust, non-cytotoxic, silica-coated CdSe quantum dots with efficient photoluminescence. Adv Mater 2005;17(13):1620–5.
[16] Osseo-Asare K, Arriagada F. Preparation of SiO2 nanoparticles in a non-ionic reverse micellar system. Colloids Surf 1990;50:321–39.
[17] Schmidt J, Guedson C, Schomäcker R. Engineering aspects of preparation of nanocrystalline particles in microemulsions. J Nanoparticle Res 1999;1(2):267–76.
[18] Zhao X, Bagwe RP, Tan W. Development of organic-dye-doped silica nanoparticles in a reverse microemulsion. Adv Mater 2004;16:173–6.
[19] Santra S, Tapec R, Theodoropoulou N, Dobson J, Hebard A, Tan W. Synthesis and characterization of silica-coated iron oxide nanoparticles in microemulsion: the effect of nonionic surfactants. Langmuir 2001;17(10):2900–6.
[20] Wang L, Wang K, Santra S, Zhao X, Hilliard LR, Smith JE, et al. Watching silica nanoparticles glow in the biological world. Anal Chem 2006;78(3):646–54.
[21] Santra S, Liesenfield B, Bertolino C, Dutta D, Cao Z, Tan W, et al. J Luminescence 2006;117:75–82.
[22] Santra S, Zhang P, Wang K, Tapec R, Tan W. Conjugation of biomolecules with luminophore-doped silica nanoparticles for photostable biomarkers. Anal Chem 2001;73(20):4988–93.
[23] Brooker LG. The theory of the photographic process. New York: Macmillan; 1971.
[24] Gibaud S, Demoy M, Andreux JP, Weingarten C, Gouritin B, Couvreur P. Cells involved in the capture of nanoparticles in hematopoieticorgans. J Pharm Sci 1996;85:944–50.
[25] Mellon PL, Windle JJ, Goldsmith PC, Padula CA, Roberts JL, Weiner RI. Immortalization of hypothalamic GnRH neurons by genetically targeted tumorigenesis. Neuron 1990;5:1–10.
[26] Radovick S, Wray S, Lee E, Nicols DK, Nakayama Y, Weintraub BD, et al. Migratory arrest of gonadotropin-releasing hormone neurons in transgenic mice. Proc Natl Acad Sci USA 1991;88:3402–6.
[27] Hays WL. Statistics. 3rd. ed. New York: Holt-Saunders International Editions; 1981.
[28] Rasband WS. ImageJ.U.S. National Institutes of Health, Bethesda, MD, USA, http://rsb.info.nih.gov/ij; 1997–2007.
[29] Legrand AP. The surface properties of silicas. New York: John Wiley; 1998.
[30] Koraiem AIM, Girgis MM, Khalil ZH, Abu El-Hamd RM. Electronic absorption spectral studies on new dimethine cyanine dyes. Dyes Pigm 1991;15(2):89–105.
[31] Kachkovski AD. Electronic properties of polymethine systems. 3: polymethine and quasi-local electron transitions. Dyes Pigm 1994;24(3):171–83.
[32] Kachkovski AD, Dekhtyar ML. Electronic properties of polymethine systems. Part 4: electronic structure of polymethine chain. Dyes Pigm 1996;30(1):43–54.
[33] Kachkovsky AD, Pilipchuk NV, Kurdyukov VV, Tolmachev AI. Electronic properties of polymethine systems. 10. Electron structure and absorption spectra of cyanine bases. Dyes Pigm 2006;70(3):212–9.
[34] Tolmachev AI, Romanov NN, Fedotov KV, Dyadyusha GG, Kachkovski AD. A study of the vinylene shifts in polymethine dyes with sulphur-containing end-groups. Dyes Pigm 1988;9(6):443–51.

[35] Sahyun MRV, Blair JT. Photophysics of a "simple" cyanide dye. J Photochem Photobiol A Chem 1997;104(1–3):179–87.
[36] Bagwe RP, Hilliard LR, Tan W. Surface modification of silica nanoparticles to reduce aggregation and nonspecific binding. Langmuir 2006;22(9):4357–62.
[37] Lackowicz JR. Principles of fluorescence spectroscopy. 3rd ed. Singapore: Springer; 2006 [a. Chapter 1, page 7–8. b. Chapter 19, page 629].
[38] Terpetschnig E, Jameson DM. Fluorescence lifetime (FLT). ISS technical notes, http://www.iss.com/resources/tech1/index.html.
[39] Dewar PJ, MacGillivray TF, Crispo SM, Smith-Palmer T. Interactions of pyrene-labeled silica particles. J Colloid Interface Sci 2000;228(2):253–8.
[40] Imhof A, Megens M, Engelberts JJ, de Lang DTN, Sprik R, Vos WL. Spectroscopy of fluorescein (FITC) dyed colloidal silica spheres. J Phys Chem B 1999;103(9):1408–15.
[41] Larson DR, Ow H, Vishwasrao HD, Heikal AA, Wiesner U, Webb WW. Silica nanoparticle architecture determines radiative properties of encapsulated fluorophores. Chem Mater 2008;20(8):2677–84.